Author/s:
Zhang, B;Gao, C;Soleimaninejad, H;White, JM;Smith, TA;Jones, DJ;Ghiggino, KP;Wong, WWH

Title:
Highly Efficient Luminescent Solar Concentrators by Selective Alignment of Donor-Emitter Fluorophores

Date:
2019-04-23

Citation:
Zhang, B., Gao, C., Soleimaninejad, H., White, J. M., Smith, T. A., Jones, D. J., Ghiggino, K. P. & Wong, W. W. H. (2019). Highly Efficient Luminescent Solar Concentrators by Selective Alignment of Donor-Emitter Fluorophores. Chemistry of Materials, 31 (8), pp.3001-3008. https://doi.org/10.1021/acs.chemmater.9b00647.

Highly Efficient Luminescent Solar Concentrators by Selective Alignment of Donor-Emitter Fluorophores

Bolong Zhang,[a,b] Can Gao,[a,b] Hamid Soleimaninejad,[a] Jonathan M. White,[b] Trevor A. Smith,[a] David J. Jones,[b] Kenneth P. Ghiggino,[a] and Wallace W. H. Wong[a,b*]

a. ARC Centre of Excellence in Exciton Science, School of Chemistry, The University of Melbourne, Parkville, Victoria, 3010, Australia.

b. School of Chemistry, Bio21 Institute, The University of Melbourne, Parkville, Victoria, 3010, Australia. E-mail: wwhwong@unimelb.edu.au.

ABSTRACT: Vertically aligning fluorophores to the surface of a waveguide is known to be an effective approach to improve the optical quantum efficiency (OQE) of luminescent solar concentrators (LSCs). While the chromophore alignment assists waveguiding of the emitted photons to the LSC edges, it also significantly reduces the light harvesting properties of the LSC. We report here a fluorophore pair consisting of a sphere-shaped energy donor and a rod-shaped emitter that was incorporated in LSCs to provide selective fluorophore alignment to address the reduced incident light absorption issue. A liquid-crystal polymer matrix was used to perpendicularly align the rod-shaped acceptors to a favorable orientation for light guiding, while the sphere-shaped donor was randomly oriented to maintain its light absorbing properties. The OQE of LSC devices with this selectively aligned donor-acceptor fluorophore system is 78% without significant loss of light harvesting capability.

1. Introduction

A luminescent solar concentrator (LSC) is a light-harvesting device containing fluorophores that absorb light over the large surface area of a planar waveguide. The resulting luminescence is guided to the device edges by total internal-reflection, where the concentrated light can be converted to electric current by a photovoltaic cell.[1] The planar geometry, together with the range of colors and transparencies possible, make LSCs particularly attractive for light harvesting applications in urban environments.[2]

The performance of LSCs is limited mainly by four aspects, namely the transmission loss due to incomplete light absorption by the fluorophores, the photoluminescence quantum yield (ϕ_{PL}) of the fluorophore, the escape-cone loss of the waveguide system, and luminescence re-absorption.[1] The transmission loss can be addressed by improving the fraction of incident light absorbed by the fluorophore, by adjusting the fluorophore concentration and/or the thickness of the LSC device. The ϕ_{PL} is related to the photophysical properties of the fluorophore system and our group and others have used a variety of strategies to improve this parameter.[2-4] The escape-cone loss refers to the re-emitted photons released from the top and bottom surfaces of the waveguide due to the refractive index change at the interface.[5, 6] Escape cone loss can be addressed by using a higher refractive index material as the waveguide, but there is a trade-off with increased reflectance of the incident light from the waveguide surface and the higher cost of high refractive index materials. The luminescence re-absorption effect does not lead to energy loss directly, but adds to the escape cone loss and the ϕ_{PL} loss in systems where there is an overlap of the absorption and emission spectra of the fluorophore.[7-9] Careful selection of a light harvesting energy donor and a highly emitting energy acceptor (the "emitter") that increases the Stokes shift has been demonstrated to reduce the re-absorption effect and improve the performance of LSCs.[10-13] The concentration of the energy donor materials is usually quite high in this case to capture the incident light, while the concentration of the emitters is adjusted to just sufficiently quench the emission from the donors. Consequently, the overall spectrum of the mixture will be dominated by the donor absorption and the emitter emission spectrum with minimum spectral overlap.

Aligning the emission transition dipole of a molecular fluorophore perpendicular to a plane, defined in Figure 1a, will bias the direction of the emitting light to be within the (*x*,*y*) plane. In the context of a LSC, aligning the emission transition dipoles of all the fluorophores perpendicular to the plane of the waveguide (Figure 1) has been shown to reduce the escape-cone loss.[14-16] However, in many cases, the absorption transition dipole of the fluorophores is parallel to the emission transition dipole leading to significant decrease in fluorophore absorption ability for light incident from the (*z*) direction, Figure 1a, resulting in LSC efficiency loss.[17, 18] This loss was reduced for a reported vertically-aligned dye system using a light diffuser layer on top of the LSC device.[15]

Selectively aligning a donor-emitter fluorophore pair is an alternative approach to overcome the drawbacks of aligning a single fluorophore species. The emitter is required to be aligned perpendicular to the plane of the waveguide to confine the re-emitted light within the waveguide, while the energy donor needs to be randomly oriented to maximally harvest the light incident on the surface of the waveguide. To fulfil this approach, two criteria need to be met: a matrix that can align the emitter perpendicular to the plane of the waveguide, but not the donor; and efficient energy transfer from the donor to the emitter (Figure 1b). With an appropriate donor-emitter energy transfer process, the emission from a high concentration of randomly distributed donor molecules can be efficiently quenched by only a small amount of emitter.[3] The high donor to emitter ratio results in a small spectral overlap reducing the luminescence re-absorption effect as discussed earlier. In addition, the low concentration of the emitter also helps to avoid the

aggregation-caused quenching effect and improves the effective ϕ_{PL} of the system.[10] In terms of the LSC performance, the selected random donor/aligned-emitter waveguide system should improve the optical quantum efficiency (OQE) of LSCs while retaining a good external quantum efficiency (EQE) by minimizing light absorption losses. OQE and EQE are defined here as the percentage of the edge output photons with relation to absorbed photons and incident photons, respectively:

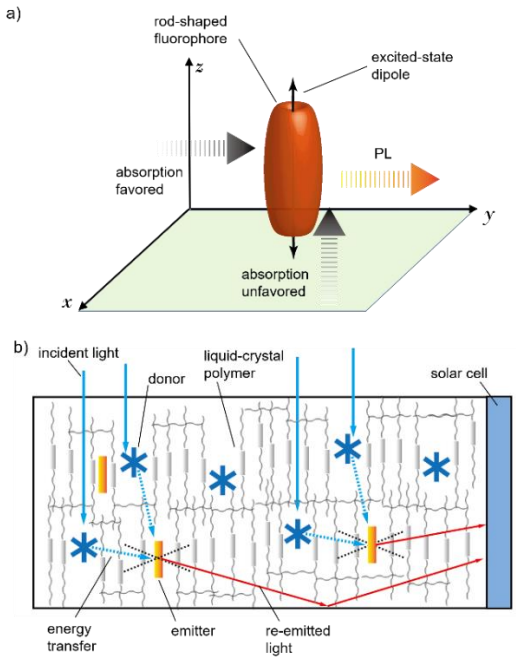

Figure 1. a) Alignment influences the observed absorption of light and emission intensity in different directions of an aligned fluorophore system; b) the wave-guiding process in a LSC device containing randomly oriented light absorbing energy donors and aligned emitters.

$$OQE = \frac{n_{edge}}{n_{abs}} \qquad \text{(Equation 1)}$$

$$EQE = \frac{n_{edge}}{n_{incident}} = OQE \times A\% \qquad \text{(Equation 2)}$$

where the n_{edge} is the number of the total edge output photons, n_{abs} is the number of incident photons that are absorbed and $n_{incident}$ refers to the number of photons incident on the waveguide surface. $A\%$ represents the percentage light absorption.

During our studies, a biomimetic light harvesting funnel system was reported whereby a selectively-aligned chromophore pair was investigated.[19] While that work provided a glimpse of this light harvesting strategy, application in LSC devices was not explored.

In this work, 9,10-diphenylanthracene (DPA) derivatives and coumarin 6 were used as energy donor and energy acceptor respectively in a selectively-aligned LSC device. The alignment of coumarin 6 in a self-assembling liquid-crystal polymer (LCP) matrix was reported previously.[15] The rod-shaped molecular structure of coumarin 6 meant that the alignment effect driven by the LCP packing was very strong. Conversely, it was envisaged that spherically-shaped molecules would not be aligned in the LCP matrix. DPA derivatives are suitable candidates as energy donor materials, due to their high ϕ_{PL}, good spectral overlap with coumarin 6 absorption and readily modifiable molecular structures. Although the DPA molecule is close to a planar-shaped structure, we proposed to install bulky substituents on the DPA structure to modify the molecular shape into an ellipsoid or even a sphere. In this way, the LCP will only drive the alignment of coumarin 6 while leaving the sphere-shaped DPA derivatives randomly oriented.

Herein, two DPA derivatives, bDPA-1 and bDPA-2, bearing isopropyl substituents on the phenyl rings, were synthesized (Figure 2a). Together with DPA, these energy donors were paired with coumarin 6, the rod-shaped emitter, as donor-emitter pairs and incorporated in both poly(methyl methacrylate) (PMMA) and the LCP thin-film waveguide matrix. LSC devices with different combinations of fluorophores and matrices were then examined revealing a benchmark experimental OQEs for the selectively aligned donor-emitter system.

2. Results and discussion

The DPA derivatives, bDPA-1 and bDPA-2, were synthesized by Suzuki-Miyaura coupling of 2,6-diisopropylphenylboronic acid pinacol ester with 9-bromo-10-phenylanthracene and 9,10-dibromoanthracene respectively (see Supporting Information for details). The absorption and emission spectra of the DPA derivatives in dilute solution were similar to each other except for the more pronounced vibronic structures for bDPA-1 and bDPA-2 (Figure 2b). As the isopropyl substituents block the free rotation of the phenyls, the vibronic structures in the spectrum of bDPA-1 and bDPA-2 were more resolved, indicating a more rigid molecular structure. As required by the donor-emitter energy transfer process, the absorption spectrum of coumarin 6 has a large degree of overlap with the emission spectrum of the DPA derivatives. In terms of reducing the re-absorption effect, the overlap of the absorption and emission spectra of the donor-emitter system was much reduced compared to the donor or emitter on their own (vide infra). The overall Stokes shift of the donor-emitter pair is approximately 75 nm.

The selectively aligned LSC devices were prepared by incorporating the donor and emitter chromophores in a self-assembled LCP matrix obtained from DIC Corporation (material number UCL018; see Supporting Information for sample preparation details). Control devices without dye alignment were fabricated by using PMMA as the polymer matrix instead of the LCP. As mentioned previously, the molecular shape is essential for selective alignment by the LCP matrix. Therefore, the donors and the emitter were all chosen or designed to have distinct molecular shapes. The shape of coumarin 6 is naturally rod-shaped while the shapes of the donors vary from planar to ellipsoid to spherical (**Figure 2c**). Molecular shape significantly influences the interaction between the LCP matrix and the fluorophores. In the donor-emitter fluorophore pair system, the concentration of the donors needed to be high to capture the incident light. However, the maximum concentration of bDPA-1 that could be included in the LCP matrix was about 50 mM while bDPA-2 precipitated at <10 mM. In contrast, samples with concentrations of up to 100 mM for DPA and coumarin 6 in the LCP matrix were prepared without any observable precipitation. This behavior indicated that the rod-shaped coumarin 6 and planar-shaped DPA interacted favorably with the LCP matrix while the sphere-shape bDPA-2 was more easily excluded from the matrix because of shape mismatch. By installing bulky groups only on one end of the DPA molecule, the shape of bDPA-1 (Figure 2c) allowed inclusion into the LCP matrix at a reasonable concentration (50 mM) for assembling a donor-emitter LSC device. Since the achievable concentration of bDPA-2 in the LCP matrix was too low, it was not examined further in this work.

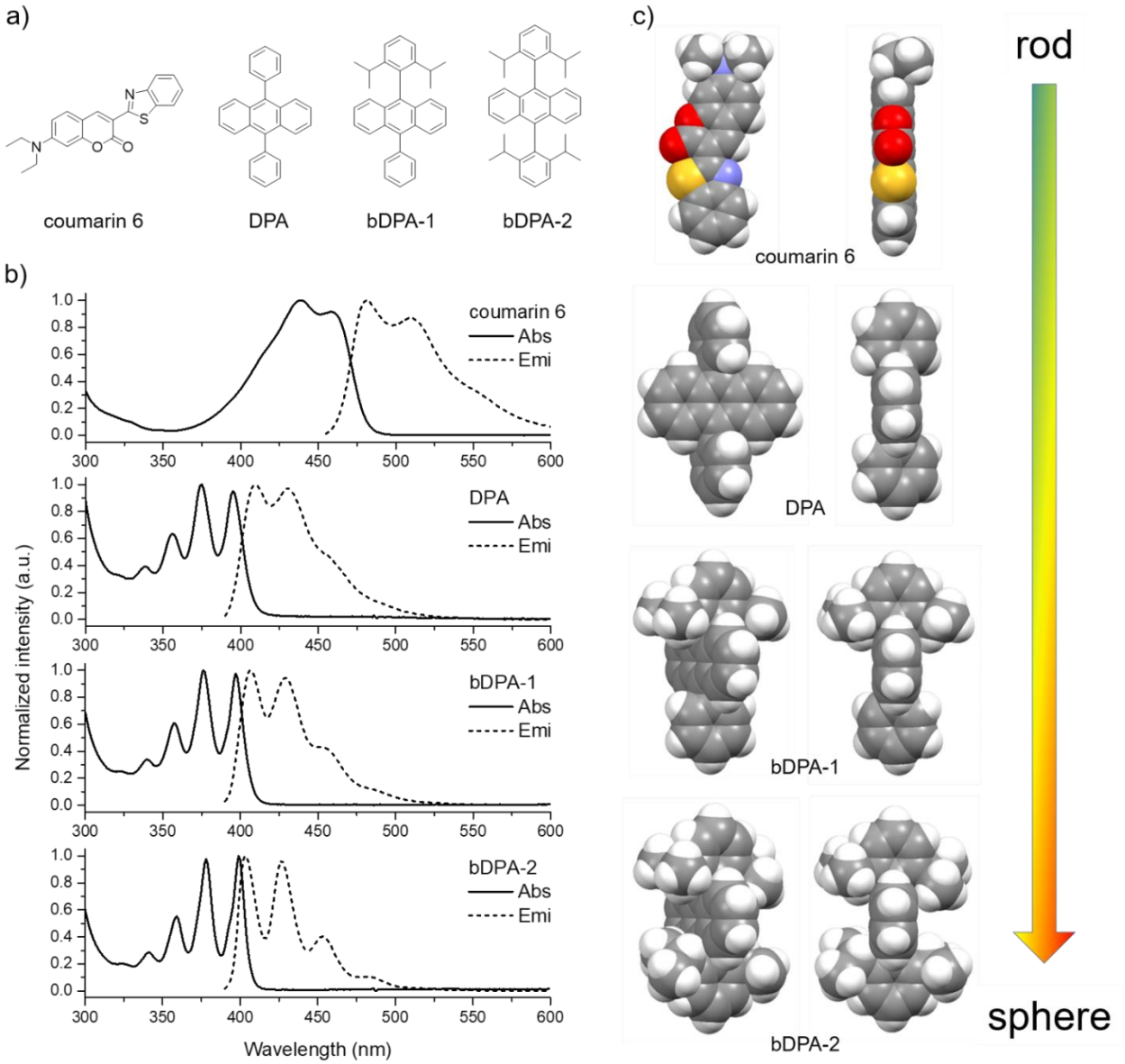

Figure 2**.** a) Chemical structures of coumarin 6 and the bDPA series, b) normalized absorption and emission spectra of the four compounds in dilute solution condition (10-5 M in toluene). Space-filling illustrations of crystal structures of coumarin 6, DPA, bDPA-1 and bDPA-2 in front and side views. The molecular shape changes from rod-like for coumarin 6 to sphere-like for bDPA-2.

Both the absorption and emission spectra of coumarin 6 showed small red-shifts in the LCP matrix compared to the spectra of the PMMA sample (Figure 3a). The spectra of the DPA derivatives also showed a very small red-shifts in LCP relative to PMMA (Figure 3b and c). The red shifts indicated a lowering of excited state energy which can be a result of the molecules residing in the more rigid LCP environment or a result of aggregation. A summary of the photophysical properties of the fluorophores in the various matrices is provided in Table 1.

The influence on the effective light absorption ability of aligning the coumarin 6 (as described in Figure 1) in the LCP matrix is shown in Figure 3a. The effective absorption ability (defined as the absorbance per molar per unit thickness) reduced markedly (~60%) in the latter case due to the increased proportion of the chromophores that have their absorption transition dipoles aligned parallel to the direction of the incident light (i.e. perpendicular to the electric field of the incident light). In comparison, the effective absorption ability by DPA and bDPA-1 only dropped by around 20% and 10% respectively (Figure 3b and 3c). The two phenyl groups of DPA must be situated out of the plane of the anthracene core making the molecule more of a thin-ellipsoid rather than planar (Figure 2c). For bDPA-1, the isopropyl substituents made the molecule even more ellipsoidal in shape with less chance of alignment by the LCP matrix. The selectivity of alignment was significant between coumarin 6 and bDPA-1.

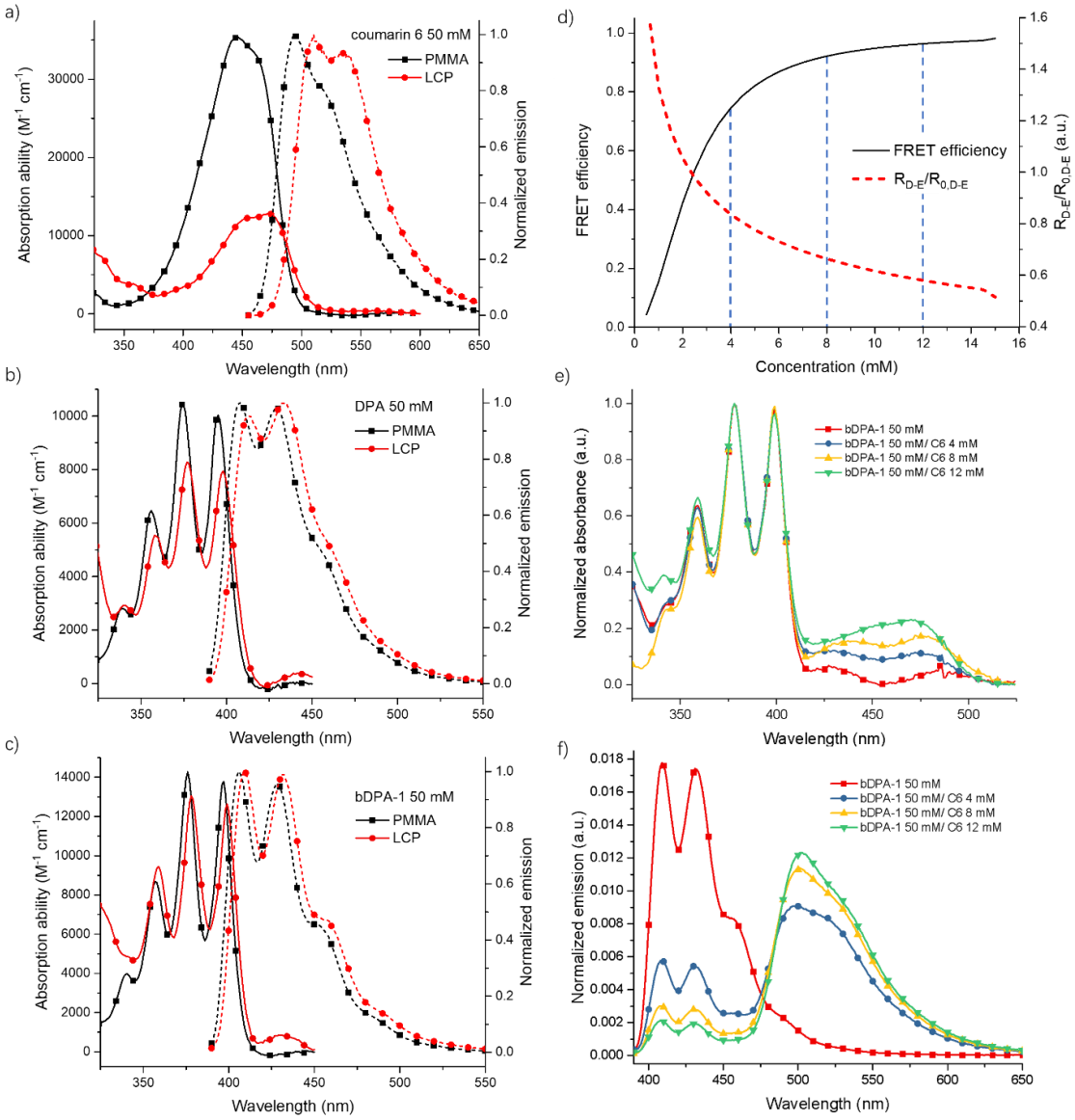

Figure 3. UV-Vis absorption spectra (solid lines) showing the observed absorption ability for light incident perpendicular to the plane of the waveguide and emission spectra (dashed) of a) coumarin 6 (C6), b) DPA and c) bDPA-1 in both PMMA and LCP thin-film matrix at 50 mM. d) The donor-to-emitter FRET efficiency (E_{D-E}) and $R_{D-E}/R_{0,D-E}$ as a function of the concentration of coumarin 6, e) normalized absorption and f) normalized (by integration) emission spectra (with excitation at 375 nm) of the bDPA-1/coumarin 6 mixture system in the LCP matrix.

The energy transfer between fluorophores that are dispersed in a solid-state matrix can be described by the Förster resonance energy transfer (FRET) mechanism.[20] The FRET process requires both dipole-dipole coupling of the fluorophores and a significant spectral overlap of the donor emission and the acceptor absorption. In an isotropic fluorophore system, the electronic coupling of dipoles increases with the fluorophore concentration as the donor-acceptor distance decreases. The emission spectra of all the DPA compounds overlapped significantly with the absorption spectrum of coumarin 6, which enabled efficient donor-emitter energy transfer pairs. The FRET critical distance (R_0, nm; the distance at which the rate for energy transfer is the same as the rate for all other excited donor relaxation processes) can be calculated via the following Förster equation[21, 22]:

$$R_0 = 0.02108 \times \left(\frac{\kappa^2 \Phi_{PL} J}{n^4}\right)^{\frac{1}{6}} \quad \text{(Equation 3)}$$

$$J = \int \varepsilon_A(\lambda) F_D(\lambda) \lambda^4 \, d\lambda \quad \text{(Equation 4)}$$

where κ^2 is the orientation factor (κ^2= 0.476 for a randomly oriented, long lifetime non-mobile donor and acceptor system in a rigid matrix[20]), Φ_{PL} refers to the PLQY of the donor fluorophore, J (nm^4 M^{-1} cm^{-1}) is the spectral overlap integral involving the area normalized emission spectrum (F_D) of the donor and the absorption coefficient (ε_A) of the acceptor, λ is the wavelength over the full spectrum, and n is the refractive index of the matrix material (assuming n = 1.5 for PMMA and n = 1.6 for LCP).

Table 1. The photophysical properties of the fluorophores in different matrices.[a]

Fluorophore	Matrix [a]	Abs_{max} (nm)	Emi_{max}(nm)	$R_{0,D-E}$(nm)[b]	Absorption ability 10^4 (M^{-1} cm^{-1})[c]
Coumarin 6	Toluene	438	481	n/a	n/a
	PMMA	445	495		3.50 ± 0.08
	LCP	472	510		1.30 ± 0.04
DPA	Toluene	375	410	4.41	n/a
	PMMA	374	408		1.04 ± 0.04
	LCP	377	434		0.830 ± 0.005
bDPA-1	Toluene	376	407	4.39	n/a
	PMMA	376	409		1.46 ± 0.06
	LCP	378	406		1.30 ± 0.03
bDPA-2	Toluene	399	403	4.37	n/a
	PMMA	n/a	n/a		n/a
	LCP	n/a	n/a		n/a

[a] The fluorophore concentration was 10^{-5} M in toluene and 50 mM in the thin-film matrix. [b] $R_{0,D-E}$ is the critical radius of the donor-to-emitter FRET process was calculated based on solution data. [c] The absorption ability is the effective absorption determined by measurement of the transmission of light incident perpendicular to the waveguide.

The calculated donor-to-emitter critical distances, $R_{0,D-E}$, are close to 4.4 nm for all donor cases (Equation 3 and 4 and Table 1). In a homogeneously dispersed system, the average intermolecular distance between the donor (high concentration) and emitter (low concentration) (R_{D-E}) is related to the average intermolecular distance of the emitters (R_{E-E}) (Equation 5, see mathematical model in Supporting Information):

$$R_{D-E} = \frac{R_{E-E}}{2\sqrt[3]{\frac{\pi}{3}}} = 0.4924\, R_{E-E} \qquad \text{(Equation 5)}$$

By using R_{D-E} and $R_{0,D-E}$, one can calculate the efficiency of the FRET process (E) (Equation 6)[23]:

$$R_{D-E} = R_{0,D-E}\left(\frac{1-E}{E}\right)^{\frac{1}{6}} \quad or \quad E = \frac{1}{\left(\frac{R_{D-E}}{R_{0,D-E}}\right)^{6}+1} \qquad \text{(Equation 6)}$$

To experimentally demonstrate the efficiency of the donor-to-emitter energy transfer in the selectively aligned system, a series of samples were prepared consisting of 50 mM of bDPA-1 with varying concentrations of coumarin 6 in the LCP matrix. According to Equation 6, the donor-to-emitter FRET efficiency (E_{D-E}) was >75% when the concentration of coumarin was 4 mM, while it increased to above 92% when the concentration reached 8 mM (Figure 3d). As shown in Figure 3e, the absorption band associated with bDPA-1 in the mixtures remained the same, while the absorption band of coumarin 6 rose proportionally with increasing concentration of coumarin 6. In contrast, the normalized emission intensity of the donor dropped dramatically with increasing coumarin 6 concentration along with the appearance of the energy acceptor emission (Figure 3f). With 8 mM of coumarin 6, the donor emission dropped to 17% of the original intensity. By considering the absorbance and emission intensities, 8 mM of coumarin 6 and 50 mM of DPA was found to be close to the optimum in terms of minimizing emission re-absorption.

Apart from donor-to-emitter energy transfer, donor-to-donor energy migration was also an important process in our light harvesting system. The donor-to-donor energy migration facilitated the transfer of energy from some donor molecules that could not couple directly to emitters under the donor-to-emitter orthogonal transition dipole orientation. At 50 mM of bDPA-1 donor, the donor-to-donor FRET critical distance ($R_{0,D-D}$) was 2.78 nm, which was smaller than the mean donor-to-donor distance (R_{D-D}) of 3.21 nm. This meant that the donor-to-donor FRET efficiency (E_{D-D}) for bDPA-1 was 34%. The residual donor emission in the presence of 8 mM coumarin emitter can be attributed to this relatively low E_{D-D} (Figure 3f).

LSC devices with coumarin 6, bDPA-1 and the bDPA-1/coumarin 6 mixtures in both PMMA and LCP matrices were fabricated by spin coating on glass slides (dimensions 1.25 × 1.25 × 0.1 cm) from toluene solutions (Figure 4a, see Supporting Information for fabrication details). The geometric gain (G) of all devices is 3 and the mean film layer thicknesses of the PMMA and LCP are 1.26 ± 0.03 mm and 1.12 ± 0.02 mm, respectively. The performance of the LSC devices is summarized in Table 2.

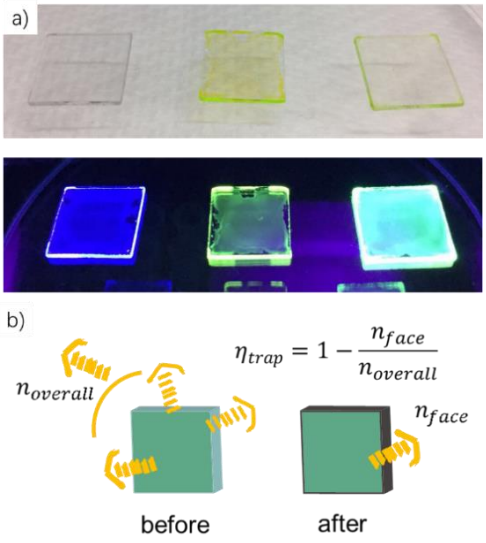

Figure 4. a) LSC devices (G = 3) fabricated based on bDPA-1, coumarin 6 and the bDPA-1/coumarin 6 mixture (left to right) in the LCP matrix. The devices are exposed to both the ambient light (top) and 365 nm UV light (bottom); b) η_{trap} of LSC devices was quantified by measuring the integrated emission of devices before and after the edges were covered by black paint. The $n_{overall}$ and n_{face} refer to the photon numbers collected from all surfaces and edges of the devices or from just the surfaces respectively.

The G is defined in this work as:

$$G = \frac{S_{surface}}{S_{edge}} \qquad \text{(Equation 7)}$$

where S_{edge} and $S_{surface}$ are the area of the edges and surface of the waveguide, respectively.

The donor-emitter fluorophore system was originally designed to increase the Stokes shift and thus minimize the re-absorption effect. By examining the overlap between the absorption spectrum and the emission spectrum (integrally normalized to 1), the re-absorption factor (F_R) of a waveguiding system can be calculated. F_R is defined by Equation 8:

$$F_R = \int_{\lambda_1}^{\lambda_2} \varepsilon_\lambda PL_\lambda d\lambda \qquad \text{(Equation 8)}$$

where ε_λ and PL_λ are the extinction coefficient and the normalized emission intensity at the given wavelength, respectively, and λ_1 and λ_2 define the spectral range.

As shown in Table 2, the F_R of all LCP based samples was smaller than in the PMMA matrix, mainly due to the red-shifted emission spectrum in the LCP matrix. For the bDPA-1/coumarin 6 mixture in either the PMMA or LCP matrix, F_R was smaller than either the donor and acceptor alone in the same matrix. This indicated that the re-absorption effect was reduced in the donor-emitter fluorophore system.

The ϕ_{PL} of coumarin 6 (50 mM) in the LCP matrix was slightly higher than in PMMA, possibly due to a better molecular dispersion (See Supporting Information for measurement details). On the other hand, the ϕ_{PL} of bDPA-1 was lower in the LCP than in PMMA. As mentioned previously, the molecular shape of bDPA-1 meant that it did not favorably interact with the LCP matrix. At this concentration, some of the bDPA-1 molecules may aggregate and form non-radiative quenching sites in the system. However, the ϕ_{PL} of the bDPA-1/coumarin 6 mixture was 98.4% in both PMMA and the LCP matrices. Compared to bDPA-1 alone, the ϕ_{PL} increase of the donor-emitter mixture was most likely a result of preferential energy trapping by the coumarin 6 emitter over non-emissive aggregate species.[10, 24]

The experimental trapping efficiencies (η_{trap}) of all LSCs were determined by comparing the emission intensity of the devices with and without the edges covered by black paint (Figure 4b, See details in the Supporting Information).[1] The η_{trap} of all samples in the PMMA matrix remained at around 72%, which was slightly lower than the theoretical limit of 75%[6, 25] for isotropic waveguide systems with 1.5 refractive index.[26] The η_{trap} of bDPA-1 in the LCP matrix was the same as in PMMA confirming that the orientation of bDPA-1 was not influenced by the LCP matrix. The η_{trap} of the donor-emitter mixture and coumarin 6-alone samples in the LCP matrix are 80.4% and 79.3% respectively. The observation that η_{trap} for these samples is greater than the isotropic limit is direct evidence for the alignment of coumarin 6 in the LCP matrix. Benefiting from the increase in both ϕ_{PL} and η_{trap}, the OQE of the bDPA-1/coumarin 6 mixture in the LCP matrix reached 78.0%, which is amongst the best experimental OQE's reported for an LSC to date.[15, 27]

The differences in the absorption and emission spectra of each fluorophore meant that the EQEs of LSCs were not directly comparable. On the other hand, the change in EQE of LSCs with the same fluorophore system but different matrix could be compared (Table 2). The EQE of bDPA-1 only samples dropped by almost two thirds (9.78% to 3.71%) from PMMA to LCP matrices, mainly because of the lower ϕ_{PL} of bDPA-1 in the LCP matrix. Although the OQE of the perpendicularly aligned coumarin 6 only samples were higher than the isotropic samples, the EQE was substantially lower (from 18.2% to 9.21%) due to the lower absorption ability of coumarin 6 in the LCP.

The EQE of the donor-emitter devices in the two matrices were similar because the improvement in η_{trap} for the LCP sample was negated by the decrease in absorption ability. Among the three LSC device pairs, the selectively aligned donor-emitter system demonstrated a high OQE without significant loss in EQE. Thus it can be envisaged that selectively aligned donor-emitter systems will be most advantageous in transparent or semi-transparent LSC applications requiring limited maximum absorbance, such as windows or tinted polymer/glass roofing. Another possible application is in stacked LSC devices.[19, 28] Since transmittance loss drops exponentially with an increase of absorbance according to the Lambert-Beer law[29], the influence from the absorbance penalty of the perpendicularly aligned system becomes less significant by stacking LSCs (Equation 9).

$$T = 0.1^A \rightarrow T^n = 0.1^{A \times n} \qquad \text{(Equation 9)}$$

The EQE of n stacked layers can be quantified by:

$$EQE_n = OQE \times (1 - T^n) = OQE \times (1 - 0.1^{A \times n}) \qquad \text{(Equation 10)}$$

where A is the observed absorbance of the devices, T is the percentage transmittance and n is the number of stacked layers.

Table 2. A summary of the LSC device performance. [a]

Fluorophores	Matrix	F_R	$\phi_{PL,observed}$ (%)[b]	η_{trap} (%)	OQE (%)	EQEc (%)
bDPA-1 50 mM	PMMA	1430	87 ± 1	73 ± 2	63 ± 2	9.78
	LCP	880	38 ± 2	70 ± 1	27 ± 2	3.71
coumarin 6 50 mM	PMMA	3030	76 ± 4	73 ± 1	55 ± 4	18.2
	LCP	600	82 ± 1	80 ± 1	66 ± 1	9.21
bDPA-1/coumarin 6	PMMA	1150	98 ± 1	73 ± 1	72 ± 2	11.2
50 mM/8 mM	LCP	420	98 ± 5	79 ± 1	78 ± 3	10.8

[a] All values in this table are averages of 9 measurements over 3 samples. All samples were measured using an integrating sphere coupled with a fluorometer, with the excitation wavelength of 375 nm for bDPA-1 and 450 nm for coumarin 6. [b] The $\phi_{PL,observed}$ values do not include the re-absorption correction. [c] EQE was calculated from OQE based on the absorbance of devices with 1 mm matrix thickness.

By stacking only 2 layers in the devices, the EQE_2 of bDPA-1/coumarin 6 in the LCP matrix can be predicted to reach 20.6%, which is higher than in the PMMA matrix (20.2%). With the same stacked structure, the EQE_2 of coumarin 6 alone in the LCP matrix (17.2%) is much lower than in the PMMA matrix (30.4%). In other words, the benefits of the selective donor-emitter alignment waveguiding system become more marked after stacking two or more layers.

3. Conclusions

In conclusion, the selective alignment of donor-emitter fluorophores in LSC devices has been experimentally demonstrated in this work. The η_{trap} of devices is enhanced from 73% for the isotropic fluorophore orientation system to 79.3% for the selective aligned fluorophore system. The resulting absorption penalty in the vertical alignment waveguide is reduced from 60% to 10% due to the presence of the isotropically dispersed bDPA-1 as the donor material. Benefiting from improvements in ϕ_{PL}, η_{trap} and the reabsorption effect, the LSC with the selectively aligned donor-emitter system showed one of the best experimental OQEs of 78% at G=3 without any noticeable decrease in EQE.

4. Experimental Section

bDPA-1: A mixture of 9-bromo-10-phenylanthracene (50 mg, 0.15 mmol), 2,6-diisopropylphenyl boronic acid pinacol ester (45 mg, 0.22 mmol), sodium tert-butyloxide (43 mg, 0.45 mmol), $Pd(OAc)_2$ (1 mg, 0.004 mmol) and 3-(t-Butyl)-4-(2,6-dimethoxyphenyl)-2,3-dihydrobenzo[d][1,3]oxaphosphole BI-DIME (3 mg, 0.009 mmol) was dissolved in degassed toluene (2 mL) and stirred at refluxing temperature under N_2 atmosphere overnight. The crude product was purified by flash chromatography (petroleum spirit 40-60 ºC) to give the target product (pale powder, 25 mg, 0.06 mmol, 40 %). ^{1}H NMR (600 MHz, 1,1,2,2-tetrachloroethane-d_2) δ 7.71 (t, *J* = 11.9 Hz, 1H), 7.66 – 7.61 (m, 1H), 7.58 (t, *J* = 6.5 Hz, 2H), 7.53 (d, *J* = 8.4 Hz, 1H), 7.42 (d, *J* = 7.8 Hz, 1H), 7.32 (dt, *J* = 14.8, 6.5 Hz, 2H), 2.15 (dd, *J* = 13.3, 6.6 Hz, 1H), 0.92 (d, *J* = 6.7 Hz, 6H). ^{13}C NMR (101 MHz, chloroform-d) δ 148.45, 139.10, 131.50, 130.36, 129.83, 128.49, 128.29, 127.38, 127.03, 126.97, 125.04, 124.66, 123.17, 30.82, 24.45. FT-IR: 3059.8, 2959.0, 2923.3, 2965.1, 1469.4, 1456.5, 1442.2, 1381.0, 1360.1, 1027.3, 941.2, 806.1, 748.6, 698.0, 664.0. HRMS (m/z): calcd. for $C_{32}H_{30}$, [M $^+$] 414.2348; found 414.23413.

bDPA-2: A mixture of dibromoanthracene (250 mg, 0.74 mmol), 2,6-diisopropylphenyl boronic acid pinacol ester (380 mg, 1.84 mmol), sodium tert-butyloxide (355 mg, 3.70 mmol), $Pd(OAc)_2$ (5 mg, 0.022 mmol) and 3-(t-Butyl)-4-(2,6-dimethoxyphenyl)-2,3-dihydrobenzo[d][1,3]oxaphosphole BI-DIME (15 mg, 0.045 mmol) was dissolved in degassed toluene (8 mL) and stirred at refluxing temperature under N_2 atmosphere overnight. The crude product was purified by flash chromatography (petroleum spirit 40-60 ºC) to give the target product (pale powder, 90 mg, 0.18 mmol, 24 %). ^{1}H NMR (400 MHz, chloroform-d_1) δ 7.61 – 7.50 (m, 3H), 7.41 (d, *J* = 7.7 Hz, 2H), 7.27 (dd, *J* = 6.4, 2.6 Hz, 2H), 2.19 (hept, *J* = 6.6 Hz, 2H), 0.91 (t, *J* = 9.9 Hz, 12H). ^{13}C NMR (101 MHz, chloroform-d) δ 148.32, 135.45, 134.77, 130.49, 128.44, 127.02, 124.83, 123.08, 30.94, 24.33. FT-IR: 3057.6, 2966.1, 2928.3, 2969.6, 1461.6, 1438.1, 1382.2, 1362.0, 941.3, 801.4, 766.9, 749.8, 673.2. HRMS (m/z): calcd. for $C_{38}H_{42}$, [M $^+$] 498.3286; found 498.32794.

X-ray crystallography: Intensity data for bDPA-1 and bDPA-2 were collected at 100 K on the MX1 beamline at the Australian Synchrotron[30], bPDI-4 was collected on an Oxford SuperNova CCD diffractometer at 130 K. The structures were solved by direct methods and difference Fourier synthesis. Thermal ellipsoid plots were generated using the program ORTEP-3 integrated within the WINGX suite of programs.

Crystal data for bDPA-1 ($C_{32}H_{30}$). M = 352.49, T = 100.00(10) K, λ= 1.54184 Å, orthorhombic, space group P-1, a = 17.2043(2), b = 8.51290(10), c = 27.5380(3) Å, α = 90° , β= 90° , γ =90° . V = 4033.17(8) Å^3, Z = 8, Dc = 1.161 Mg/m^3, μ(Mo-Kα) 0.485 mm^{-1}, F(000) = 1520, crystal size 0.205 x 0.135x 0.022 mm^3. 49342 reflections measured to a maximum θ = 78.057° , 4295 independent reflections (R_{int} = 0.1494), the final R was 0.0728 [I > 2σ(I)] and wR(F2) was 0.1909 (all data).

Crystal data for bDPA-2 ($C_{38}H_{42}$). M = 498.71, T = 100.00(10) K, λ= 0.71073 Å, triclinic, space group P-1, a = 8.4236(2), b = 8.8483(3), c = 10.6311(3) Å, α = 88.521(2) ° , β= 76.573(2) ° , γ = 67.212(3) ° . V = 708.75(4) Å^3, Z = 1, Dc = 1.168 Mg/m^3, μ(Mo-Kα) 0.065 mm^{-1}, F(000) = 270, crystal size 0.698 x 0.36x 0.167 mm^3. 14483 reflections measured to a maximum θ = 36.968° , 6561 independent reflections (R_{int} = 0.0263), the final R was 0.0532 [I > 2σ(I)] and wR(F2) was 0.1643 (all data).

Thin-film LSC device preparation

Thin-film sample preparation for absolute PLQY measurement: All the glass (MENZEL-GLÄSER Microscope Slides, 76 × 26 mm) slides used in fabricating LSC devices were cut to 1.25 cm × 1.25 cm × 0.1 cm, cleaned by sonicating sequentially in $CHCl_3$, acetone, NaOH (a.q.), distilled water, isopropanol and acetone, then dried using a strong flow of N_2.

The LSC devices were prepared by spin coating 20 μL casting solution on top of the above-mentioned glass slides. The spin-coating conditions were 2000 rpm (2000 rpm/s) for 1 minute to deposit the PMMA thin-film matrix and 1200 rpm (1200 rpm/s) for 15 seconds to deposit the LCP thin-film matrix. The casting solutions were prepared by dissolving the required quantity of fluorophores in either PMMA solution (8% w/w in toluene) or UCL-018 solution (relative density 1.2, 20% w/w in toluene). The correct quantities of added fluorophores were determined by measuring aliquots from stock solutions (5 mM in toluene) using an automatic pipette, the solvent was removed using a vacuum drying oven (60ºC, 35 mbar), before adding to the matrix solution. After spin-coating, the LSC devices were placed in a dry N_2 atmosphere for 1 minute and exposed to a UV-lamp (180 nm) for 30 seconds to cure the LCP matrix.

Absolute PLQY measurements of all samples were performed according to the experimental approach described elsewhere[31, 32] using the integrating sphere accessory (F3018, Horiba Jobin Yvon) for a Fluorolog®-3 fluorimeter. The angle of the excitation beam to the normal of the sample surface can be modified using the variable sample holder. All spectra for the absolute quantum yield measurements were corrected for the light source noise, wavelength sensitivity and the transmittance of the filters. The photon counts of all the measurements on the Fluorolog®-3 fluorimeter were within the linear response range of the detector (2 × 10^6 cps).

The trapping efficiency (η_{trap}) measurements of all samples were performed according to the experimental approach described elsewhere[31, 32] using the same conditions described in the absolute PLQY measurement process. The spectra of all samples were recorded with the device edges both covered and not covered by black paint. The η_{trap} can be calculated by the following equation:

$$\eta_{trap} = 1 - \frac{PL_{surface}}{PL_0}$$

where, $PL_{surface}$ and PL_0 are the integrated emission spectra from the samples with and without the edges being covered by the black paint respectively. To eliminate the influence of the black paint on the responsivity of the integrating-sphere, a white paint was coated over the outside of the black painted surfaces.

Supporting Information. Supporting Information is available online. This material is available free of charge via the Internet at http://pubs.acs.org. [CCDC 1887085, CCDC 1887086, CCDC 1294096, CCDC 113041 contains the supplementary crystallographic data for this paper. These data can be obtained free of charge from The Cambridge Crystallographic Data Centre via www.ccdc.cam.ac.uk/data_request/cif.]

AUTHOR INFORMATION

Corresponding Author

* Wallace W. H. Wong
ARC Centre of Excellence in Exciton Science, School of Chemistry, The University of Melbourne, Parkville, Victoria, 3010, Australia. E-mail: wwwong@unimelb.edu.au.

Author Contributions

The manuscript was written through contributions of all authors. All authors have given approval to the final version of the manuscript.

ACKNOWLEDGMENT

This work was made possible by support from the Australian Renewable Energy Agency which funds the project grants within the Australian Centre for Advanced Photovoltaics (ACAP). WWHW was supported by an ARC Future Fellowship (FT130100500). TAS, KPG and WWHW are also supported by the ARC Centre of Excellence in Exciton Science (CE170100026). The authors are also thankful to Dr Yasuhiro Kuwana, DIC Corporation, for providing the liquid crystal polymer matrix for this study.

REFERENCES

(1) Tummeltshammer, C.; Taylor, A.; Kenyon, A. J.; Papakonstantinou, I., Losses in Luminescent Solar Concentrators Unveiled. *Sol. Energy Mater. Sol. Cells* **2016,** *144*, 40-47.
(2) Hong, Y.; Lam, J. W. Y.; Tang, B. Z., Aggregation-Induced Emission. *Chem. Soc. Rev.* **2011,** *40*, 5361-5388.
(3) Banal, J. L.; Zhang, B.; Jones, D. J.; Ghiggino, K. P.; Wong, W. W., Emissive Molecular Aggregates and Energy Migration in Luminescent Solar Concentrators. *Acc. Chem. Res.* **2017,** *50*, 49-57.
(4) Meinardi, F.; McDaniel, H.; Carulli, F.; Colombo, A.; Velizhanin, K. A.; Makarov, N. S.; Simonutti, R.; Klimov, V. I.; Brovelli, S., Highly Efficient Large-Area Colourless Luminescent Solar Concentrators Using Heavy-Metal-Free Colloidal Quantum Dots. *Nat. Nanotechnol.* **2015,** *10*, 878-885.
(5) McDowall, S.; Butler, T.; Bain, E.; Scharnhorst, K.; Patrick, D., Comprehensive Analysis of Escape-Cone Losses from Luminescent Waveguides. *Appl. Opt.* **2013,** *52*, 1230-1239.
(6) Debije, M. G.; Verbunt, P. P.; Rowan, B. C.; Richards, B. S.; Hoeks, T. L., Measured Surface Loss from Luminescent Solar Concentrator Waveguides. *Appl. Opt.* **2008,** *47*, 6763-6768.
(7) Gutierrez, G. D.; Coropceanu, I.; Bawendi, M. G.; Swager, T. M., A Low Reabsorbing Luminescent Solar Concentrator Employing π - Conjugated Polymers. *Adv. Mater.* **2016,** *28*, 497-501.
(8) Olson, R. W.; Loring, R. F.; Fayer, M. D., Luminescent Solar Concentrators and the Reabsorption Problem. *Appl. Opt.* **1981,** *20*, 2934-2940.
(9) Erickson, C. S.; Bradshaw, L. R.; McDowall, S.; Gilbertson, J. D.; Gamelin, D. R.; Patrick, D. L., Zero-Reabsorption Doped-Nanocrystal Luminescent Solar Concentrators. *ACS Nano* **2014,** *8*, 3461-3467.
(10) Zhang, B. L.; Soleimaninejad, H.; Jones, D. J.; White, J. M.; Ghiggino, K. P.; Smith, T. A.; Wong, W. W. H., Highly Fluorescent Molecularly Insulated Perylene Diimides: Effect of Concentration on Photophysical Properties. *Chem. Mater.* **2017,** *29*, 8395-8403.
(11) Banal, J. L.; Soleimaninejad, H.; Jradi, F. M.; Liu, M.; White, J. M.; Blakers, A. W.; Cooper, M. W.; Jones, D. J.; Ghiggino, K. P.; Marder, S. R.; Smith, T. A.; Wong, W. W. H., Energy Migration in Organic Solar Concentrators with a Molecularly Insulated Perylene Diimide. *J. Phys. Chem. C* **2016,** *120*, 12952-12958.
(12) Currie, M. J.; Mapel, J. K.; Heidel, T. D.; Goffri, S.; Baldo, M. A., High-Efficiency Organic Solar Concentrators for Photovoltaics. *Science* **2008,** *321*, 226-228.
(13) Davis, N. J. L. K.; MacQueen, R. W.; Jones, S. T. E.; Orofino-Pena, C.; Cortizo-Lacalle, D.; Taylor, R. G. D.; Credgington, D.; Skabara, P. J.; Greenham, N. C., Star-Shaped Fluorene–Bodipy Oligomers: Versatile Donor–Acceptor Systems for Luminescent Solar Concentrators. *J. Mater. Chem. C* **2017,** *5*, 1952-1962.
(14) MacQueen, R. W.; Cheng, Y. Y.; Clady, R. G.; Schmidt, T. W., Towards an Aligned Luminophore Solar Concentrator. *Opt. Express* **2010,** *18 Suppl 2*, A161-6.
(15) Mulder, C. L.; Reusswig, P. D.; Velázquez, A. M.; Kim, H.; Rotschild, C.; Baldo, M. A., Dye Alignment in Luminescent Solar Concentrators: I. Vertical Alignment for Improved Waveguide Coupling. *Opt. Express* **2010,** *18*, 90.
(16) Eisfeld, A.; Briggs, J. S., Dye Aggregates in Luminescent Solar Concentrators. *Phys. Status Solidi A* **2018,** *215*, 1700634.
(17) MacQueen, R. W.; Schmidt, T. W., Molecular Polarization Switching for Improved Light Coupling in Luminescent Solar Concentrators. *J. Phys. Chem. Lett.* **2013,** *4*, 2874-2879.
(18) ter Schiphorst, J.; Kendhale, A. M.; Debije, M. G.; Menelaou, C.; Herz, L. M.; Schenning, A. P. H. J., Dichroic Perylene Bisimide Triad Displaying Energy Transfer in Switchable Luminescent Solar Concentrators. *Chem. Mater.* **2014,** *26*, 3876-3878.
(19) Pieper, A.; Hohgardt, M.; Willich, M.; Gacek, D. A.; Hafi, N.; Pfennig, D.; Albrecht, A.; Walla, P. J., Biomimetic Light-Harvesting Funnels for Re-Directioning of Diffuse Light. *Nat. Comm.* **2018,** *9*, 666.
(20) Lakowicz, J. R., *Energy Transfer*. Springer, Basel, **1999**; p 367-349.
(21) Demchenko, A. P., *Introduction to Fluorescence Sensing*. Springer Science & Business Media, Basel, **2008**.
(22) Medintz, I.; Hildebrandt, N., *Fret-Förster Resonance Energy Transfer: From Theory to Applications*. John Wiley & Sons, Hoboken, **2013**.
(23) Pietraszewska - Bogiel, A.; Gadella, T. W. J., Fret Microscopy: From Principle to Routine Technology in Cell Biology. *J. Microsc.* **2011,** *241*, 111-118.
(24) Zhang, B.; Banal, J. L.; Jones, D. J.; Tang, B.; Ghiggino, K. P.; Wong, W. W. H., Aggregation-Induced Emission-Mediated Spectral Downconversion in Luminescent Solar Concentrators. *Mater. Chem. Front.* **2018,** *2*, 615-619.
(25) Hernandez-Noyola, H.; Potterveld, D. H.; Holt, R. J.; Darling, S. B., Optimizing Luminescent Solar Concentrator Design. *Energy Environ. Sci.* **2011,** *5*, 5798-5802.

(26) Dienel, T.; Bauer, C.; Dolamic, I.; Brühwiler, D., Spectral-Based Analysis of Thin Film Luminescent Solar Concentrators. *Sol. Energy* **2010,** *84*, 1366-1369.
(27) Benjamin, W. E.; Veit, D. R.; Perkins, M. J.; Bain, E.; Scharnhorst, K.; McDowall, S.; Patrick, D. L.; Gilbertson, J. D., Sterically Engineered Perylene Dyes for High Efficiency Oriented Fluorophore Luminescent Solar Concentrators. *Chem. Mater.* **2014,** *26*, 1291-1293.
(28) Carlotti, M.; Ruggeri, G.; Bellina, F.; Pucci, A., Enhancing Optical Efficiency of Thin-Film Luminescent Solar Concentrators by Combining Energy Transfer and Stacked Design. *J. Lumin.* **2016,** *171*, 215-220.
(29) *IUPAC. Compendium of Chemical Terminology, 2nd Ed. (the "Gold Book").* Blackwell Scientific Publications, Oxford, **1997**.
(30) Cowieson, N.; Aragao, D.; Clift, M.; Ericsson, D. J.; Gee, C.; Harrop, S. J.; Mudie, N.; Panjikar, S.; Price, J. R.; Riboldi-Tunnicliffe, A., Mx1: A Bending-Magnet Crystallography Beamline Serving Both Chemical and Macromolecular Crystallography Communities at the Australian Synchrotron. *J. Synchrotron Radiat.* **2015,** *22*, 187-190.
(31) Porres, L.; Holland, A.; Pålsson, L.-O.; Monkman, A. P.; Kemp, C.; Beeby, A., Absolute Measurements of Photoluminescence Quantum Yields of Solutions Using an Integrating Sphere. *J. Fluoresc.* **2006,** *16*, 267-273.
(32) Würth, C.; Grabolle, M.; Pauli, J.; Spieles, M.; Resch-Genger, U., Relative and Absolute Determination of Fluorescence Quantum Yields of Transparent Samples. *Nat. Protoc.* **2013,** *8*, 1535-1550.

SYNOPSIS TOC